doi:10.1038/nature09618

1 Model for the evolution of conduit cross-sections: equation (1) of the main article

As in the main article, I use the term 'conduit' below to describe all types of water filled openings at the glacier bed through which water can flow. I assume that these come in two flavours, channels and cavities. My aim in constructing equation (1) of the main article is to describe the dynamics of channels and cavities in a single model, in order to be able to capture the switch between these different types of conduits dynamically. The equation takes the form

$$\frac{\mathrm{d}S}{\mathrm{d}t} = c_1 Q\Psi + u_b h - c_2 N^n S, \tag{1}$$

where S is conduit cross-sectional area, Q is water discharge (volume per unit time), Ψ is hydraulic potential gradient along the conduit, u_b is sliding velocity, h is a representative height of protrusions on the glacier bed causing the opening of cavities, N is effective pressure and c_1 and c_2 are constants given by material properties and geometry that I define below. In terms of the ice overburden pressure p_i and water pressure p_w in the channel, N is defined as

$$N = p_i - p_w, \tag{2}$$

while the hydraulic gradient Ψ is given by a downslope component of gravity and a water pressure gradient along the conduit, i.e.,

$$\Psi = -\rho_w g \frac{\partial b}{\partial s} - \frac{\partial p_w}{\partial s} \tag{3}$$

where ρ_w is water density, g acceleration due to gravity, b bed elevation, p_w water pressure and s is distance along the conduit. In terms of N, this can be written as

$$\Psi = \Psi_0 + \frac{\partial N}{\partial s}. \tag{4}$$

where $\Psi_0 = -\frac{\partial p_i}{\partial s} - \rho_w g \frac{\partial b}{\partial s}$ is a background hydraulic gradient controlled by ice thickness and bed slopes.

The terms on the right-hand side of (1) signify that conduit cross-sectional area evolves over time in response to melting of the walls due to dissipation in the conduit (represented by the first term), opening of an ice-bed gap due to sliding over bed protrusions (the second term) and viscous creep closure (the third term). These are the principal mechanisms by which subglacial conduits are known to open and close[1,2]. The form of equation (1) is inspired by previous work on cavities that involved the three mechanisms described above.[3] I proceed to show next that equation (1) agrees with established theories for drainage through individual channels and cavities, unifying them into a single model.

1.1 Channels

The basic theory for R-channels was described by Röthlisberger[4] and Nye[5], and I repeat only the essential components here to motivate equation 1. For simplicity, consider a semicircular channel cross-section of radius r and cross-sectional area $S = \pi r^2/2$. The rate at which the channel expands or contracts is determined by the difference between the rate of wall melt and creep closure.

The rate of creep closure driven by the difference between ice overburden pressure p_i and channel pressure p_w can be computed as[6] $2An^{-n}N^nS$, where A and n are parameters in Glen's law[7] (typically $n = 3$ and $A \sim 10^{-24}\,\mathrm{Pa}^{-3}\,\mathrm{s}^{-1}$), and $N = p_i - p_w$ is effective pressure. Wall melt is caused by dissipation in the conduit. $Q\Psi$ is the rate of work done by the hydraulic gradient per unit length of conduit. Assuming insignificant changes in kinetic energy, this is the rate of dissipation. If dissipated energy is immediately turned into latent heat, the rate of wall melting is $Q\Psi/(\rho_i L)$, where ρ_i is ice density and L is latent heat of fusion per unit mass of ice. Then

$$\frac{\mathrm{d}S}{\mathrm{d}t} = \frac{Q\Psi}{\rho_i L} - 2An^{-n}N^nS. \tag{5}$$

Equation (5) applies to conduits large enough to be unaffected by bedrock roughness. For large S (and hence large Q), the gap opening term $u_b h$ can be dropped from equation (1), which then becomes $\mathrm{d}S/\,\mathrm{d}t = c_1 Q\Psi - c_2 N^n S$. This agrees with (5) if I take $c_1 = 1/\rho_i L$ and $c_2 = 2An^{-n}$.

There are different parameterizations for turbulent discharge Q. Here I use a Darcy-Weisbach law for turbulent water flow[8] relating flow velocity u to Ψ as $\rho_\mathrm{w} f u|u| = (\pi + 2)r\Psi$, where $f \sim 0.1$ is a friction factor and $(2 + \pi)r$ is the wetted perimeter of the channel. With $Q = Su = \pi r^2 u/2$, this yields

$$Q = c_3 S^\alpha |\Psi|^{-1/2}\Psi \tag{6}$$

where $\alpha = 5/4$ and $c_3 = 2^{1/4}\sqrt{\pi + 2}/[\pi^{1/4}\sqrt{\rho_\mathrm{w} f}]$

1.2 Cavities

A complete continuum model of cavities takes the form of a complicated viscous contact problem.[9,10,11,12] However, Walder[3] captured the qualitative behaviour of cavities, consistent with solutions of the contact problem, by using a much simpler steady-state model similar to equation 1. In this vein, I show here that (1) reproduces the key features of cavity dynamics predicted by more complicated models.

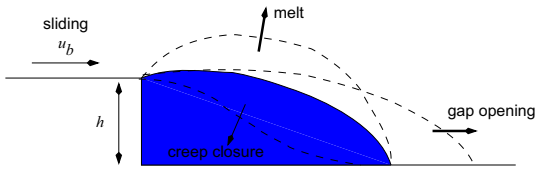


Figure 1: The basic processes that contribute to the opening and closing of a conduit in the lee of a bedrock step. Opening occurs by sliding over the bedrock step and dissipation-driven melting, closing happens through viscous creep driven by the difference between overburden and water pressure.

Figure 1 illustrates how gap opening, melt and creep closure affect cavity size. For small cavities, heat dissipation can be neglected in comparison with gap opening $u_b h$ and creep closure. Dropping the term $c_1 Q\Psi$ in (1), the steady-state cavity cross-section is given by

$$S = \frac{u_b h}{c_2 N^n} \tag{7}$$

In the seminal paper by Kamb[10], cavity shapes are computed for step-shaped bed protrusions and a Newtonian ice rheology ($n = 1$). From Kamb's equations (4) and (5), cross-section S behaves as

$$S = \frac{1}{16}\sqrt{\frac{\eta u_b h^3}{\pi N}} \tag{8}$$

where η is viscosity ($= (2A)^{-1}$ if $n = 1$). There is qualitative but not quantitative agreement here: in both cases, cavity size increases with sliding velocity and step height, and decreases with effective pressure, but with different quantitative dependences. The reason is that Kamb assumes shallow cavities, while my closure rate applies to cavities with $O(1)$ aspect ratios: Kamb's downward velocity of the cavity roof scales as $w \sim Nl/\eta$. The rate at which downward velocity reduces the cavity cross-section is $\sim wl \sim Nl^2/\eta \sim NS^2/(\eta h^2)$ if $S \sim hl$. In other words, to agree fully with Kamb's model, I would have to replace my equation (1) by

$$\frac{\mathrm{d}S}{\mathrm{d}t} = c_1 Q\Psi + u_b h - c_2 N^n S^2/h^2, \tag{9}$$

in which case (7) would become

$$S = \sqrt{\frac{u_b h^3}{c_2 N^n}}. \tag{10}$$

in agreement with (8) if $n = 1$. However, Kamb's shallow cavity assumption breaks down when $l \sim h$ so $S \sim h^2$, when my closure rate may be more appropriate. I persist

with (1) because it simplifies the task of modelling channels and cavities in the same model, on the understanding that cavities must not be too shallow (so my model may be most appropriate for the 'N-channel' like cavities of Weertman[13], see also Kamb's figure 4.).

Kamb also finds that, at fixed hydraulic gradient, there is a critical effective pressure N_c below which no steady cavity shape is possible and a runaway enlargement of the cavity due to wall melt will occur. The same effect was also predicted by Walder's[3] simpler model. This runaway occurs if, for some fixed Ψ and N, the right-hand side of (1) is always positive regardless of S. With Q given by (6), the right-hand side of (1) can then be minimized with respect to S. If the minimum is positive, Kamb's runaway melt must occur. It can be shown that this is the case when

$$N < N_c = \frac{\alpha^{1/n}(c_1 c_3)^{1/(\alpha n)}(u_b h)^{(\alpha-1)/(\alpha n)}|\Psi|^{3/(2\alpha n)}}{c_2^{1/n}(\alpha-1)^{(\alpha-1)/(\alpha n)}} \tag{11}$$

Again, this agrees qualitatively but not quantitatively with the critical effective pressure predicted by the stability parameter Ξ in equation (17) of Kamb's paper[10]: for instance, as in Kamb's paper, my N_c increases with step height h and hydraulic gradient Ψ. This can again be attributed the differences to differing aspect ratios.

There is one important caveat to the unification of channel and cavity dynamics in a single model here. Channels can change their orientation, and can be expected to align themselves in the direction that maximizes the hydraulic gradient in the channel. In general, this can be expected to be close to the flow direction, as both hydraulic gradient and ice flow are strongly driven by ice surface slope. Cavities by contrast are tied to the locations of bedrock steps, and in general their direction must be at least somewhat oblique to the ice flow direction. The tortuosity of a flow path through cavities can therefore be expected to be larger than that of a channel. The model advocated above would need modification in order to account for changes in conduit alignment. This is left for future work.

2 Channels versus cavities: instability and channelization

I will now define 'channels' and 'cavities' in my model, which makes no *a priori* distinction between the two. This allows us to confirm the predictions made about channelization in the main article. Combining (1) and (6) gives

$$\frac{\mathrm{d}S}{\mathrm{d}t} = c_1 c_3 S^\alpha |\Psi|^{3/2} + u_b h - c_2 N^n S. \tag{12}$$

Consider at the steady states of (12). For $N < N_c$, there are no steady state solutions, while for $N > N_c$, (12) admits two equilibria. Mathematically, Kamb's runaway conduit enlargement by melting should therefore not be viewed as an instability, but as a bifurcation: it does not describe a positive feedback leading to the growth of a conduit that is perturbed away from an equilibrium size (which would

be an instability), but the disappearance of an equilibrium as the system parameter N drops below a critical value N_c (panel (d) of figure 2). I will show below that the formation of a channelized drainage system is driven by an instability, and that this is subtly different from Kamb's runaway melting.

First, I define channels and cavities. Assume that $N > N_c$, so that there are two equilbria for S. The larger of these equilibria can be identified as a 'channel': as with classical R-channels, the conduit cross-section S at this equilibrium point increases with effective pressure N. This occurs because the equilibrium represents a balance between wall melt and creep closure, with gap opening due to sliding playing a minor role (figure 2). An increase in effective pressure then leads to an increase in closure rate, and in steady state this must be offset by an increase in melt rate. The latter is achieved by widening the conduit. Channel cross-section, and therefore discharge, therefore increase with increasing effective pressure for this equilibrium conduit. I take this property to be the definition of a 'channel-like' equilibrium (or, for short, of a channel).

The smaller equilibrium can be identified as a 'cavity': as in other models[14,3,9,10,11,12], cavity size decreases with increasing effective pressure. This is because creep closure approximately balances gap opening due to sliding at the smaller equilibrium, while melting plays a lesser role. For a fixed u_b, the gap opening rate remains constant, and so must the creep closure rate if equilibrium is maintained. An increase in effective pressure tends to increase the creep closure rate $c_2 N^n S$, and this must be offset by a simultaneous reduction in S. Hence channel cross-section and discharge decrease with increasing effective pressure. I take this as the definition of a 'cavity-like' equilibrium (or a cavity for short).

For fixed effective pressure $N = \bar{N}$ and hydraulic gradient Ψ, the two equilibria also have different stability properties: if perturbed to slightly larger conduit size, the channel equilibrium undergoes unstable enlargement by wall melting[5,15]. Increasing S slightly beyond the larger equilibrium in panel (a) of figure 2 leads to melt exceeding closure rate. Further enlargement of the conduit ensues (see figure 3). It is this instability that drives the initial stages of a subglacial flood or *jökulhlaup*[5].The cavity equilibrium by contrast is stable to perturbations: a slight increase in size S leads to closure exceeding melt and S will shrink back towards equilibrium.

It can be shown mathematically that the jökulhlaup instability of channels under fixed N and Ψ is intrinsically tied to the fact that equilibrium channel size increases with N. To simplify my notation, I define an opening and a closure rate through

$$v_m(S,\Psi) = u_b h + c_1 c_3 S^\alpha |\Psi|^{3/2}, \qquad v_c(S,N) = c_2 N^n S. \tag{13}$$

and a water flux given by

$$q(S,\Psi) = c_3 S^\alpha |\Psi|^{-1/2}\Psi, \tag{14}$$

so that (12) becomes

$$\frac{\mathrm{d}S}{\mathrm{d}t} = v_m(S,\Psi) - v_c(S,N). \tag{15}$$

If I denote the fixed effective pressure by $\bar{N}$ and a corresponding equilibrium conduit size by $\bar{S}$, then

$$v_m(\bar{S},\Psi) = v_c(\bar{S},\bar{N}). \tag{16}$$

Perturbing this slightly by putting $S = \bar{S} + S'$ and linearizing (15), I find

$$\frac{\mathrm{d}S'}{\mathrm{d}t} = (v_{m,S} - v_{c,S})\, S', \tag{17}$$

where

$$v_{m,S} = \left.\frac{\partial v_m}{\partial S}\right|_{S=\bar{S}}, \qquad v_{c,S} = \left.\frac{\partial v_c}{\partial S}\right|_{S=\bar{S},N=\bar{N}}, \qquad v_{c,N} = \left.\frac{\partial v_c}{\partial N}\right|_{S=\bar{S},N=\bar{N}}, \tag{18}$$

and S' evolves as

$$S'(t) = S'(0) \exp\left[(v_{m,S} - v_{c,S})\, t\right]. \tag{19}$$

Unstable growth therefore occurs when

$$v_{m,S} - v_{c,S} > 0. \tag{20}$$

The physics behind this statement is simply that instability occurs if a small increase S' in conduit size leads to a larger increase $v_{m,S}S'$ in melt rate than the increase $v_{c,S}S'$ in closure rate.

But (20) is equivalent to requiring that the equilibrum conduit size $\bar{S}$ defined by (16) increases with effective pressure $\bar{N}$: applying the chain rule to (16) gives

$$v_{m,S}\frac{\partial \bar{S}}{\partial \bar{N}} = v_{c,S}\frac{\partial \bar{S}}{\partial \bar{N}} + v_{c,N}, \tag{21}$$

and hence

$$\frac{\partial \bar{S}}{\partial \bar{N}} = \frac{v_{c,N}}{v_{m,S} - v_{c,S}}. \tag{22}$$

But closure rate v_c always increases with effective pressure, so $\partial\bar{S}/\partial\bar{N} > 0$ if and only if (20) is satisfied. By extension, it also follows that steady state flux increases with effective pressure $\bar{N}$ if and only if (20) holds: denoting

$$q_S = \left.\frac{\partial q}{\partial S}\right|_{S=\bar{S}}, \tag{23}$$

I have $q_S > 0$ and, if $\bar{Q} = q(\bar{S}, \Psi)$,

$$\frac{\partial \bar{Q}}{\partial \bar{N}} = \frac{q_S v_{c,N}}{v_{m,S} - v_{c,S}}. \tag{24}$$

Hence $\partial\bar{Q}/\partial\bar{N}$ has the same sign as $v_{m,S} - v_{c,S}$.

In a real hydraulic system, conditions of fixed Ψ and N are never actually present, and are only closely approximated at the beginning of a jökulhlaup, when a large and as yet undrained water reservoir keeps N constant[5]. Runaway is generally limited by the fact that a limited amount of water is available and water discharge cannot increase indefinitely. I will show next that, under conditions of steady water input rather than of fixed N a very similar instability leads to the concentration of flow into a few large channels as predicted in the main article.

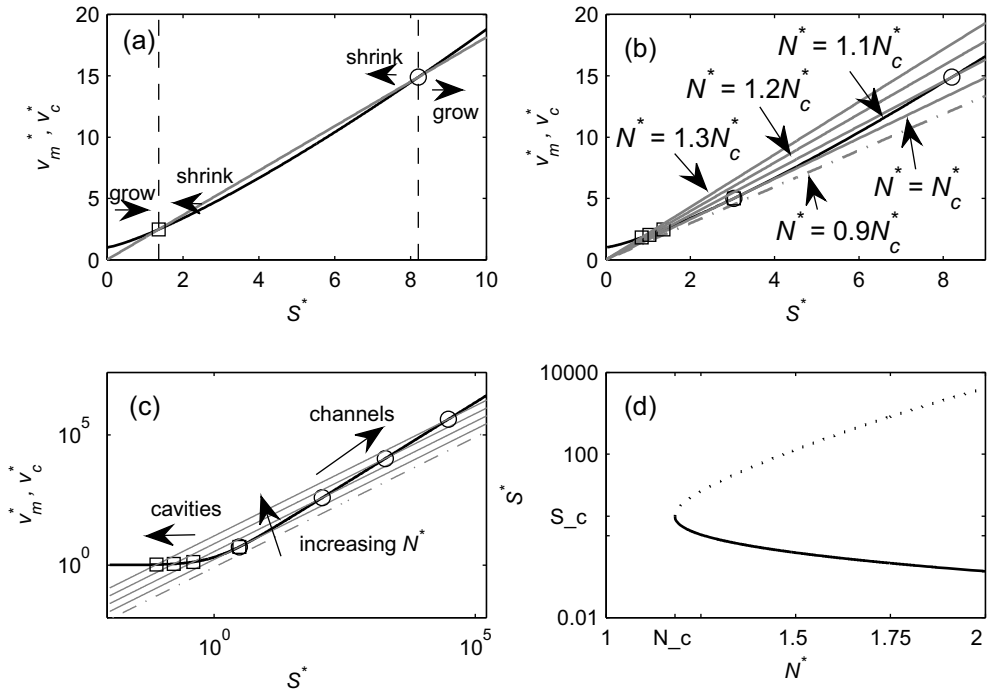


Figure 2: Steady states and the competition between conduit opening and closing mechanisms. Panel (a): Opening rate $v_m = u_b h + c_1 Q\Psi = u_b h + c_1 c_3 S^\alpha |\Psi|^{3/2}$ (solid black line) and closing rate $v_c = c_2 N^n S$ (grey line) against S for fixed N and Ψ. Variables here are normalized as $v_m^* = v_m/[v]$, $v_c^* = v_c/[v]$, $S^* = S/[S]$ where $[v] = u_b h$, $[S] = [u_b h/(c_1 c_3 |\Psi|^{3/2})]^{1/\alpha}$. With this choice of scales and $t^* = t[v]/[S]$, $N^* = N/[N]$, $[N] = c_1^{-(\alpha-1)/(\alpha n)} c_2^{-1/n} c_3^{1/(\alpha n)} (u_b h)^{(\alpha-1)/(\alpha n)} \Psi^{3/(2\alpha n)}$, (12) becomes $\mathrm{d}S^*/\,\mathrm{d}t^* = S^{*\alpha} + 1 - S^* N^{*n}$. Equlibrium conduits are points of intersection of the graphs. The larger equlibrium (circle) is unstable to perturbations, the smaller (square) is stable. Panel (b): Change in equilibria as N^* is changed: grey lines show v_c^* for different N^* as indicated , where $N_c^* = N_c/[N] = 1.1815$. The smaller (cavity) equilibrium decreases, the larger (channel) equilibrium increases with N^*. The equilibria exist only for $N^* \geq N_c^*$. Panel (c): same as panel (b), on a log scale, with $N^* = 0.9N_c^*$ (dot-dashed grey line), N_c^*, $1.1N_c^*$, $1.2N_c^*$ and $1.3N_c^*$ (solid grey) . Panel (d) Equlibrium S^* against N^* for channels (dotted) and cavities (solid grey line). Note that channel size increases very rapidly with effective pressure. Also note that a saddle-node bifurcation occurs at $N^* = N_c^*$, with no solution below N_c^*, and two above.

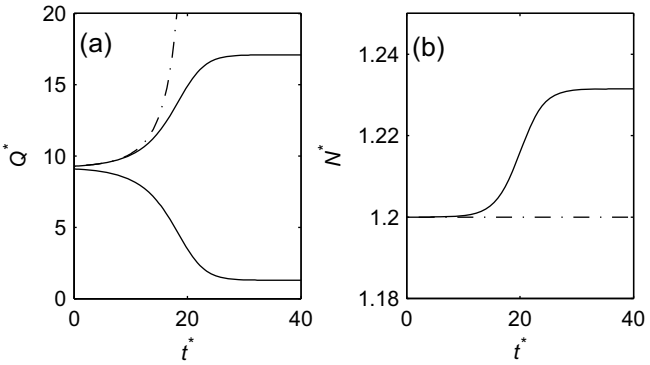


Figure 3: Instabilities in parallel conduit flow. Panel (a): Scaled flux $Q^* = Q/[Q] = S^{*\alpha}$ against scaled time t^*, where $[Q] = u_b h/(c_1\Psi)$, other scales as in figure 2. Solid lines: discharge in two conduits in parallel carrying a fixed mean flux $\bar{Q}^* = 9.2$. Over time, the conduit that is slightly larger initially grows at the expense of the smaller one. Dashed line: a single conduit subject to fixed effective pressure $N^* = 1.2$, with the same initial size as the larger conduit in parallel. The single conduit initially grows at the same rate as the larger conduit in paralllel, but then blows up in size while the conduits in parallel reach steady states. In fact, it can be shown that the single conduit blows up in some finite time t_c with $S^* \sim (t_c^* - t^*)^{-1/(\alpha-1)}$ close to blow-up. Panel (b): Corresponding effective pressure $N^* = N/[N]$ against t^*. Solid line: effective pressure in the conduits in parallel. N^* here increases as the larger conduit grows, allowing it to stabilize. Dashed line: effective pressure in the single conduit is held constant, allowing it blow up.

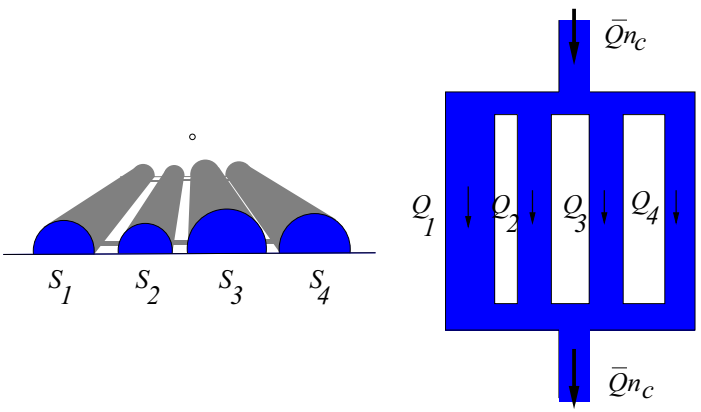


Figure 4: Geometry of a conduit array. Perspective view (left) and schematic view from above (right). The illustration on the right shows an array with $n_c = 4$ in which one conduit ($i = 1$) is larger than the others, which are of equal size; this picture corresponds to the analysis in section 2.1.2.

2.1 Stability analysis: conduits in parallel

To understand the stability of a drainage system consisting of many conduits better, consider an array of n_c conduits in parallel, carrying a fixed mean discharge $\bar{Q}$ per conduit (figure 4). Suppose that the conduits are subjected to the same fixed hydraulic gradient $\Psi > 0$ (i.e., assume that the last term on the right-hand side of (4) can be ignored). Also assume that the conduits are laterally connected: by this, I mean that the conduits are at the same effective pressure N (which is not fixed but can vary to keep the mean discharge in the conduits fixed) and that the conduits can freely exchange water between themselves. This allows larger conduits to discharge water that cannot be accomodated by smaller ones. These assumptions are likely to be a good representation of drainage under a glacier forced by a given surface melt input (i.e., not by an upstream reservoir) and with a hydraulic gradient controlled by glacier surface and bed slopes.[7] I will use this set-up to confirm the statement in the main text that the onset of channelization corresponds to a critical mean discharge Q_c per conduit being reached, and that the return to a non-channelized state corresponds to mean discharge dropping below a lower critical value $Q_m < Q_c$, leading to hysteresis in the drainage system.

Labelling the conduits by subscripts i, the array can be modelled as

$$\frac{\mathrm{d}S_i}{\mathrm{d}t} = v_m(S_i, \Psi) - v_c(S_i, N), \tag{25a}$$

$$\frac{1}{n_c}\sum_{i=1}^{n_c} q(S_i, \Psi) = \bar{Q}. \tag{25b}$$

At fixed hydraulic gradient, the constraint on total discharge in the second equation fixes effective pressure $N(t)$: effective pressure changes over time to ensure that the conduit sizes $S_i(t)$ collectively always allow a mean discharge $\bar{Q}$ driven by the fixed hydraulic gradient Ψ. I consider this dynamical system close to its equilibrium configurations and perform a linear stability analysis (see also Creyts and Schoof[16] for a similar stabilty analysis applied to water sheets under ice streams).

2.1.1 Initially nearly uniform state: equation (3) of the main article

Suppose that all conduits are initially close to the same size $\bar{S}$, which I refer to as an unchannelized drainage configuration. $\bar{S}$ is given implicitly by

$$q(\bar{S}, \Psi) = \bar{Q} \tag{26}$$

and at an effective pressure $\bar{N}$ given implicitly by

$$v_c(\bar{S}, \bar{N}) = v_m(\bar{S}, \Psi). \tag{27}$$

Linearizing in the perturbations $S_i' = S_i - \bar{S}$, $N' = N - \bar{N}$, these perturbations evolve as

$$\frac{\mathrm{d}S_i'}{\mathrm{d}t} = v_{m,S}S_i' - v_{c,S}S_i' - v_{c,N}N', \tag{28a}$$

$$\sum_{i=1}^{n_c} q_S S_i' = 0 \tag{28b}$$

where $v_{m,S}$, $v_{c,S}$ and q_S are defined as in (18) and (23), and

N' can be eliminated from (28a): summing (28a) over i in (28a) and using $\sum_{i=1}^{n_c} S_i' = 0$ from (28b) with constant q_S, I find in fact that $N' = 0$, and hence that

$$S_i' = S_i'(0) \exp\left[(v_{m,S} - v_{c,S})\, t\right]. \tag{29}$$

Growth of the perturbations and hence instability therefore occurs again when (20) is satisfied. The mechanism is also the same: a small positive perturbation S' in conduit size leads to a greater increase $v_{m,S}S'$ in melt rate than in closure rate $v_{c,S}S'$. The difference here is that, to keep mean flux fixed, growth in one channel requires shrinkage in another. This affects the nonlinear evolution of the instability: rather than the channel blowing up, the growth of the instability is limited by the fact that total discharge must remain fixed (figure 3)

I have already shown that the criterion (20) is satisfied if and only if the conduits are channel-like. This confirms my assertion in the main article that a system of uniformly-sized conduits is stable if and only if they are all cavity-like. If they are channel-like, some of the conduits will grow at the expense of others, and the flow will become concentrated.

By (24), the instability therefore occurs if and only if discharge in the steady-state conduits increases with effective pressure. Equally, from (24), the instability occurs if and only if

$$\partial \bar{N}/\partial \bar{Q} > 0, \tag{30}$$

i.e., if and only if effective pressure $\bar{N}$ in the conduits increases with the mean discharge $\bar{Q}$. In other words, effective pressure in channel-like steady-state conduits increases with discharge, and channel-like conduits in parallel are unstable to the concentration of flow into a single channel.

Next, I use this to demonstrate that the instability occurs if and only if $\bar{Q} > Q_c$, with Q_c given by equation (3) in the main article. In steady state, (13), (14), (26) and (27) combine to give

$$\bar{N}^n = \frac{c_1 \bar{Q} \Psi + u_b h}{c_2 c_3^{-1/\alpha} \bar{Q}^{1/\alpha} \Psi^{-1/(2\alpha)}}. \tag{31}$$

By differentiating, it is easy to show that $\bar{N}$ therefore decreases with increasing $\bar{Q}$ for

$$\bar{Q} < Q_c = \frac{u_b h}{c_1 (\alpha - 1) \Psi}. \tag{32}$$

and increases with $\bar{Q}$ otherwise (panel (a) of figure 5: note that Q_c is the steady state flux at the critical effective pressure N_c). It follows that equally-sized conduits in steady state are channel-like and therefore unstable in the sense above when $\bar{Q} > Q_c$, and cavity-like and stable for $\bar{Q} < Q_c$.

2.1.2 Stability of channelized configurations

Uniformly-sized conduits flowing in parallel are only stable if cavity-like, and this is possible only below a critical mean water discharge Q_c. Suppose now that the drainage

system is not composed of uniform cavity-like conduits (for instance if $\bar{Q} > Q_c$), but settles into a different steady state, in which not all conduits are of the same size. For our array of laterally-connected conduits, I show that only a single conduit can be channel-like in this steady state. This will be referred to as a channelized drainage configuration. I also show that channelized drainage configurations are stable if and only if steady state effective pressure $\bar{N}$ in the conduits increases when mean discharge $\bar{Q}$ is increased. These conditions for stable channelized drainage configurations allow me to confirm in section 2.1.3 that stable channelized configurations always exist for $\bar{Q} > Q_c$ (when the unchannelized configuration is unstable) and also for a range $Q_m < \bar{Q} < Q_c$ below the critical discharge Q_c, leading to hysteresis.

Consider an array in which some conduits are at channel-like equilibria while others are at cavity-like equilibria. If there is more than one channel-like conduit, it is easy to see that the same instability as before will occur once more. To show this, perturb only the sizes of the channel-like conduits away from equilibrium, keeping the cavity-like ones fixed. This gives a situation perfectly analogous to section 2.1.1 with channel-like conduits flowing in parallel, giving rise to instability.

In a stable steady state, the array can therefore contain at most one channel-like conduit. Let the cross-sectional area of this conduit in steady state be $\bar{S}^+$, and $\bar{S}^-$ for the cavity-like conduits. The two steady state conduit sizes and effective pressure $\bar{N}$ are determined by the three equations

$$\begin{aligned} v_m(\bar{S}^+, \Psi) &= v_c(\bar{S}^+, \bar{N}), && \text{(33a)} \\ v_m(\bar{S}^-, \Psi) &= v_c(\bar{S}^-, \bar{N}), && \text{(33b)} \\ (n_c - 1)q(\bar{S}^-, \Psi) + q(\bar{S}^+, \Psi) &= n_c \bar{Q}. && \text{(33c)} \end{aligned}$$

Define

$$v^{\pm}_{m,S} = \left.\frac{\partial v_m}{\partial S}\right|_{S=\bar{S}^{\pm}}, \qquad v^{\pm}_{c,S} = \left.\frac{\partial v_c}{\partial S}\right|_{S=\bar{S}^{\pm},N=\bar{N}^{\pm}}, \qquad v^{\pm}_{c,N} = \left.\frac{\partial v_c}{\partial N}\right|_{S=\bar{S}^{\pm},N=\bar{N}^{\pm}}, \qquad q^{\pm}_{S} = \left.\frac{\partial q}{\partial S}\right|_{S=\bar{S}^{\pm}},$$

the $+$ and $-$ signs being applied consistenly on both sides of each equation. In addition to (33), I require that $\bar{S}^+$ be channel-like and $\bar{S}^-$ be cavity-like. From (22), this is equivalent to

$$v^+_{m,S} - v^+_{c,S} > 0, \qquad v^-_{m,S} - v^-_{c,S} < 0. \tag{34}$$

Using $i = 1$ to label the channel-like conduit, I have $S_1 = \bar{S}^+$ and $S_i = \bar{S}^-$ for $i > 1$ at equilibrium. This equilibrium can be perturbed as

$$S_i = \begin{cases} \bar{S}^+ + S'_1 & i = 1, \\ \bar{S}^- + S'_i & i = 2, \ldots, n_c \end{cases} \tag{35}$$

Linearizing (25),

$$\begin{aligned} \frac{\mathrm{d}S'_1}{\mathrm{d}t} &= \left(v^+_{m,S} - v^+_{c,S}\right) S'_1 - v^+_{c,N} N' \quad \text{for } i = 1, && \text{(36a)} \\ \frac{\mathrm{d}S'_i}{\mathrm{d}t} &= \left(v^-_{m,S} - v^-_{c,S}\right) S'_i - v^-_{c,N} N' \quad \text{for } i > 1, && \text{(36b)} \\ 0 &= q^+_S S'_1 + \textstyle\sum_{i=2}^{n_c} q^-_S S'_i \quad , && \text{(36c)} \end{aligned}$$

As before, I can eliminate N' by summing (36b) over i and substituting in (36c):

$$N' = \frac{q_S^+}{(n_c - 1)v_{c,N}^- q_S^-}\left[\frac{\mathrm{d}S_1'}{\mathrm{d}t} - (v_{m,S}^- - v_{c,S}^-)S_1'\right] \tag{37}$$

Substituting into (36a) and looking for solutions of the form $S_1' = S_1'(0)\exp(\lambda t)$ yields

$$\lambda = \frac{n_c q_s^- v_{c,N}^-(v_{m,S}^+ - v_{c,S}^+) + q_S^+ v_{c,N}^+(v_{m,S}^- - v_{c,S}^-)}{n_c v_{c,N}^- q_S^- + v_{c,N}^+ q_S^+}, \tag{38}$$

which replaces the simpler (29).

Stable states have negative λ. Since flux q and closure rate v_c increase with increasing S and N respectively, the sign of λ is the sign of the numerator in (38), and stability requires

$$n_c q_S^- v_{c,N}^-(v_{m,S}^+ - v_{c,S}^+) + q_S^+ v_{c,N}^+(v_{m,S}^- - v_{c,S}^-) < 0. \tag{39}$$

Next, I derive a simpler stability criterion. From (33) the effective pressure $\bar{N}$ is in general a function of mean flux $\bar{Q}$. I will show next that (39) is equivalent to

$$\frac{\partial \bar{N}}{\partial \bar{Q}} > 0. \tag{40}$$

In other words, a channelized steady state is stable if and only if effective pressure in the array of conduits increases with mean discharge through the conduits.

Applying the chain rule to (33), one finds

$$\begin{aligned}\frac{\partial \bar{Q}}{\partial \bar{N}} &= \frac{\partial \bar{Q}}{\partial \bar{S}^+}\frac{\partial \bar{S}^+}{\partial \bar{N}} + \frac{\partial \bar{Q}}{\partial \bar{S}^-}\frac{\partial \bar{S}^-}{\partial \bar{N}} \\ &= \frac{1}{n_c} q_S^+ \frac{v_{c,N}^+}{v_{m,S}^+ - v_{c,S}^+} + q_S^- \frac{v_{c,N}^-}{v_{m,S}^- - v_{c,S}^+} \\ &= \frac{q_S^+ v_{c,N}^+(v_{m,S}^- - v_{c,S}^-) + n_c q_S^- v_{c,N}^-(v_{m,S}^+ - v_{c,S}^+)}{(v_{m,S}^+ - v_{c,S}^+)(v_{m,S}^- - v_{c,S}^-)}.\end{aligned} \tag{41}$$

Recall that $v_{m,S}^- - v_{c,S}^- < 0$ and $v_{m,S}^+ - v_{c,S}^+ > 0$. Hence $\partial \bar{Q}/\partial \bar{N} > 0$ if and only if the numerator in the last line of (41) is negative. From (39), this is equivalent to $\lambda < 0$. Since $\partial \bar{N}/\partial \bar{Q} = \left(\partial \bar{Q}/\partial \bar{N}\right)^{-1}$, (40) follows.

2.1.3 Numerical steady state solutions for the conduit array: hysteresis under changes in discharge

I have derived stability criteria for channelized and unchannelized steady states for an array of conduits in parallel: in short, effective pressure *decreases* with increasing discharge in unchannelized drainage (equation (30)), and *increases* with discharge in channelized drainage (equation (40)).

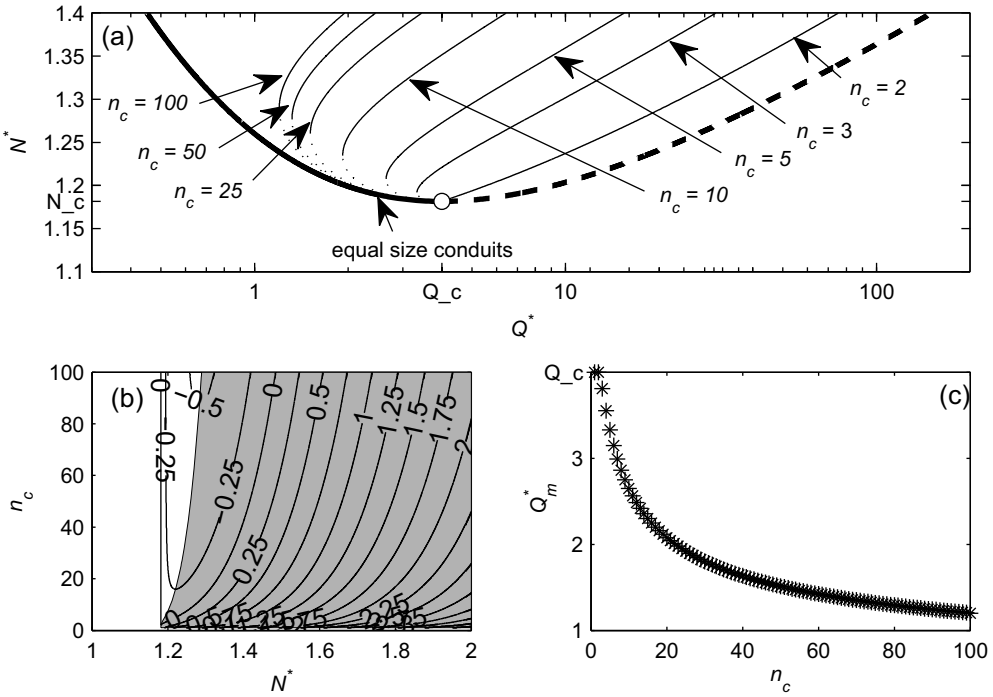


Figure 5: Steady state effective pressure against discharge in conduit arrays. Panel (a): scaled effective pressure $\bar{N}^* = \bar{N}/[N]$ against mean discharge $\bar{Q}^*/[Q]$ in an array of conduits in parallel. Scales $[N]$ and $[Q]$ are defined in figure 2. The heavy curve corresponds to (31) (an unchannelized configuration). The bifurcation point (Q_c^*, N_c^*) (shown as a circle) separates the stable (solid) and unstable (dotted) branches of the curve. Thin curves show channelized configurations (n_c indicated by arrows). Unstable branches ($\partial\bar{N}^*/\partial\bar{Q}^* < 0$) are dotted, stable branches ($\partial\bar{N}^*/\partial\bar{Q}^* > 0$) solid lines. Note that the bifurcation at $Q^* = Q_c^*$ is in fact a transcritical birfucation: the unstable branches can be continued to the right of Q_c^*, where they represent configurations consisting of $(n_c - 1)$ channels and one cavity. Panel (b): contours of $\bar{Q}^*$ against $\bar{N}^*$ and n_c for channelized configurations, contour labels show $\log(\bar{Q}^*)$. Panel (c): minimum discharge $Q_m^*(n_c) = Q_m(n_c)/[Q]$ in a channelized configuration against conduit number n_c.

Next, I compute steady states for unchannelized and channelized systems, and use the criteria above to identify which of these steady states are stable. For unchannelized systems, (13), (14), (26) and (27) lead to the relationship (31) between discharge and effective pressure. This relationship does not depend on the number n_c of conduits in the system. Panel (a) of figure 5 shows this relationship as a heavy line. The stable portion is shown as a solid line, and the unstable portion as a dashed line.

For a channelized system, an analogous relationship can only be computed numerically from (33), and in general the result will depend on n_c. Panel (a) of figure 5 shows a number of these relationships as thin lines with the corresponding n_c indicated by arrows. In general, these curves have an unstable portion shown as a dashed line, and a stable portion shown as a solid line.

Figure 5 shows that a stable channelized system exists for $\bar{Q} > Q_c$, regardless of the number of conduits n_c. For $n_c > 2$, the channelized system is even stable for discharges below Q_c: the stable branch of the channelized $\bar{N}$–$\bar{Q}$ relationship extends to a lower critical point $Q_m < Q_c$, whose value depends on n_c. This confirms the statements in the main text that a single channel will grow at the expense of other nearby ones, and that this process of channelization is generally irreversible: If I begin with some mean discharge $\bar{Q} < Q_m$, the drainage system will initially settle into an unchannelized steady state. If $\bar{Q}$ is subsequently increased, the system remains unchannelized until Q exceeds Q_c. Then instability sets in and the system will transition into a channelized state. If $\bar{Q}$ is subsequently reduced again, the system will remain channelized until $\bar{Q}$ drops below the lower critical value Q_m. In other words, the system can undergo hysteresis under changes in discharge, and this hysteresis is associated with transitions from unchannelized to channelized states and back again.

In panel (b) of figure 5, I show a corresponding contour plot of $\bar{Q}$ as a function of $\bar{N}$ and conduit number n_c for channelized configurations. The stable region where $\partial\bar{Q}/\partial\bar{N} > 0$ is shown in grey. The minimum effective pressure in a channelized configuration clearly increases with conduit number. Panel (c) shows the minimum mean discharge $Q_m(n_c)$ above which an array with a single channel can be stable. The minimum mean discharge $Q_m(n_c)$ decreases with increasing channel number n_c in the array. The physics responsible is simple: in a channelized system (with $n_c - 1$ cavities and one channel), discharge Q in the channel-like conduit is not equal to mean discharge $\bar{Q}$, but larger because flow is concentrated into this conduit. This allows the channel to maintain itself even at low mean discharge, and the effect is amplified when the mean discharge of many conduits is concentrated into a single channel.

In a real drainage system, the number n_c of conduits that can be considered as 'connected' (i.e. subject to the same effective pressure and hydraulic gradient) therefore becomes important. For conduits that are fixed in space (by the location of bedrock protrusions), the number n_c is related to the spacing between the main channelized conduits in the system. Naturally, separate channels must be associated with lateral water pressure gradients: if these are absent, all drainage elements are at the same effective pressure as in the array model above, and there can be only a single channel. I will argue below that the lateral spacing is therefore controlled by

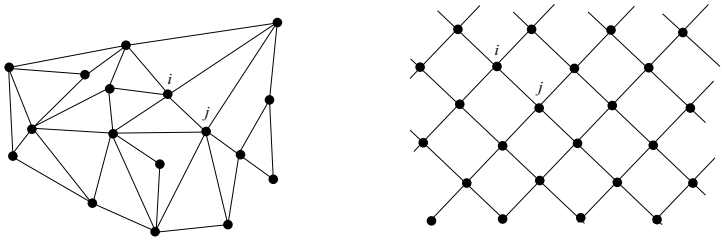


Figure 6: Drainage network geometry. A network of drainage consists of conduits (straight lines) linking nodes (solid circles). The figure on the left shows a general, unstructured network, the figure on the right a lattice network of the type used in the simulations here. The formulation of the network model in (42)–(49) is not specific to a lattice network.

lateral pressure gradients driving water flow into the main channelized conduits. This can only be captured by a more elaborate model than the simple array of conduits above.

3 Network of conduits

3.1 Model description

The array of conduits considered above was useful in understanding the process of channelization, but is too simple to represent a real drainage system. It does not account for lateral variations in effective pressure, or edge effects. As we have seen, without lateral variations in effective pressure, there can be only one stable channel, and more complicated drainage networks cannot be modeled in this way.

To address this, I consider here a two-dimensional network of conduits, inspired by the earlier work on simple hydraulic circuits by Clarke[8] and by similar models in river dynamics[17,18]. The network consists of a set of nodes i connected by conduits. I use this network model to simulate the spontaneous formation of channelized drainage networks in the main article.

The cross-section S_{ij} of the conduit connecting nodes i and j then evolves according to (1):

$$\frac{\mathrm{d}S_{ij}}{\mathrm{d}t} = c_1 Q_{ij}\Psi_{ij} + u_b h - c_2 N_{ij}^n S_{ij}. \tag{42}$$

where Q_{ij} is the flux through the conduit from i to j, Ψ_{ij} is hydraulic gradient and N_{ij} is effective pressure in the conduit. I define water pressure $p_{w,i}$, bed elevation b_i and ice thickness h_i at each node. From (4), the hydraulic gradient of the conduit ij is then given by

$$\Psi_{ij} = \Psi_{0,ij} + \frac{N_j - N_i}{L_{ij}}, \tag{43}$$

where

$$\Psi_{0,ij} = \frac{1}{L_{ij}}\left(\rho_i g(h_i - h_j) + \rho_w g(b_i - b_j)\right) \tag{44}$$

is determined by ice and bed geometry only. Effective pressure in the conduit is taken as the mean over the effective pressures at the neighbouring nodes,

$$N_{ij} = \frac{N_i + N_j}{2}, \tag{45}$$

and flux in the conduit is given by

$$Q_{ij} = c_3 S_{ij}^{\alpha} \left|\Psi_{ij}\right|^{-1/2} \Psi_{ij}. \tag{46}$$

To conserve mass in the system, one can write

$$\frac{\mathrm{d}V_i}{\mathrm{d}t} = -\sum_j Q_{ij} + m_i, \tag{47}$$

where the sum is over nodes j connected to node i. V_i is the amount of water storage at node i and m_i water supply to the node. I ignore water storage in the conduits themselves here, as residence times in conduits are generally small compared with the timescale for conduit evolution.[19]

In general there is storage of water at the bed, for instance in large cavities that do not control the flow of water but act as water reservoirs,[20] and in basal crevasses. For the parameter choices presented in this paper, realistic water storage makes little quantitative difference, and the results shown in the main article all correspond to $V_i \equiv 0$. In figure 7 and figure 11, I show some results with water storage to confirm this. I propose two water storage models: one has a 'dead-end' or storage cavity connected to each node, in which water can be stored but through which it does not flow. In analogy (1), I put

$$\frac{\mathrm{d}V_i}{\mathrm{d}t} = u_b h_V n_V L_V - c_3 N_i^n V_i \tag{48}$$

where h_v is a representative height, L_V a representative width of the bed protrusions in whose lee these storage cavities form, and n_V the number of such storage cavities connected to each network node. Storage cavities then play the role of the large cavities in Kamb's[10] theory, with cavity-like conduits playing the same role as Kamb's 'orifices'.

An alternative model has water stored in basal crevasses, and storage is a function of effective pressure that depends on their hypsometry:[8] for instance for a parallel-sided slot of base area A, we get

$$V_i = \frac{A p_{w,i}}{\rho_w g} = \frac{A(\rho g h_i - N_i)}{\rho_w g}. \tag{49}$$

The disadvantage of using a network of the type described above is primarily that all conduit locations remain fixed in space. Physically, these locations can be pictured as bedrock steps that allow linked cavities to form (i.e., as the locations of Kamb's[10] 'orifices'). It is physically realistic to assume that cavities do remain tied to these locations, but, as Kamb already points out, channels can detach themselves

from these bedrock steps. The effect of such detachment is unclear, but it seems likely that it can lead to lower tortuosity in a network that contains channels, as these can straighten themselves out, whereas the tortuosity of a network of cavities is controlled by bedrock undulations. Another limitation can arise if, as is the case below, a structured network such as a lattice is used for simulations. In that case, significant grid effects can be visible in the computed results. In the case of the lattice-type network used in this paper, there is a tendency for secondary channels to form at 45° to the downslope direction. A more practical limitation is, however, computational. By contrast with 'porous medium' models for subglacial drainage[21], my approach requires individual drainage conduits to be resolved. For a given domain size, computational resources then limit their density. Similarly, for a given density of conduits, only a limited domain size can be modelled.

3.2 Simulations

A square lattice network with $N_{\mathrm{nodes}} = 2 \times 10^4$ edges (conduits) oriented at 45° to the down-glacier direction was used in my simulations. I assume a flat bed inclined at fixed angle $\alpha = 3°$ to the horizontal. To represent glacier geometry (which enters through h_i), I assume the profile adopted by a plastic glacier with yield stress 10^5 Pa resting on a slope α.[22] Zero effective pressure is imposed on the drainage system at the glacier margin, while inflow is prescribed at the upstream boundary, and periodic boundary conditions apply at the sides of the domain to suppress edge effects. As a domain size, I use an ice mass 20 km wide and 10 km long, inspired by the edge of a larger ice cap rather than a valley glacier, in which the location of drainage channels may be controlled strongly by bed topography. The remaining parameter values are shown in table 1. The model is solved using a backward Euler step.

To prevent conduits becoming excessively large near the margin, where N is small, I amend (1) slightly by limiting the gap-opening term when S becomes large. I put

$$u_b h = u_b h_0 \left\{ 1 - \frac{1}{2} \tanh \left[\beta (S_0 - S) \right] \right\}.$$

In more complete models for cavity formation, a similar effect occurs as neighbouring cavities limit each other's growth (see e.g. the wave cavity in Kamb[10] and the periodic beds in Fowler[9] and Schoof[11]).

Mean discharge through the system is determined by the rate of water input m_i in (47). Unless stated otherwise, I use spatially uniform m_i, expressed as an equivalent rate of water supply m per unit area of the bed (see table 2):

$$m = m_i N_{\mathrm{nodes}} / A_{\mathrm{domain}},$$

where A_{domain} is the domain size. For $m = 0.33$ cm day^{-1}, the system always evolves to a state in which no channels are present (panels a1,a2 in figure 7). For $m = 0.66$ cm day^{-1} and 1 cm day^{-1}, the system does not evolve channels if it starts in a state that is nearly uniform, with only small perturbations imposed, but channels remain if the system is started with an already channelized initial condition (panels

Parameter	symbol	Value
Density of ice	ρ_i	910 kg m^{-3}
Density of water	ρ_w	1000 kg m^{-3}
Glen's law exponent	n	3
Glen's law fluidity coefficient	A	6×10^{-24} Pa^{-3} s^{-1}
Darcy-Weisbach friction factor	f	3.75×10^{-2}
Latent heat of fusion	L	3.35×10^{5} J kg^{-1}
Sliding velocity	u_b	30 m year^{-1}
Bed step ('Kamb orifice') height	h	0.1 m
Melt opening parameter	c_1	$1/(\rho_i L)$
Closure parameter	c_2	$1An^{-n}$
Flux parameter	c_3	$2^{1/4}\sqrt{\pi+2}/[\pi^{1/4}\sqrt{\rho_\mathrm{w} f}]$
Storage cavity step height	h_V	1 m
Length of storge cavity	L_V	70 m
Number of storage cavities per network node	n_V	140

Table 1: Parameter values used in simulations. The storage parameters are intended to give an upper bound on likely storage at the bed, and are used only in some of the simulations as indicated. Otherwise, I assume no storage in the drainage system.

Row in figure 7	m (cm day^{-1})	$\bar{Q}$ (m^3 s^{-1})
a	0.33	0.38
b	0.66	0.76
c	1	0.115
d	2	0.23
e	10	1.15

Table 2: Water input rates in the simulations in figure 7. The mean discharge per conduit is based on each conduit having a 1 km^2 catchment taken over the entire domain.

c1,c2 and d1,d2 in figure 7). The local pressure minima in each channel in (b1,b2) and (c1,c2) are sufficient to suck in enough water to maintain the channels open, but the discharge in the system is too small to cause channels to form spontaneously from an initially nearly uniform system. For $m = 2$ cm day^{-1} and 10 cm day^{-1}, the system always evolves channels.

These results agree with the theory of section 2. For a 3° slope with conduits oriented at 45° to downslope, the contribution of gravity to the hydraulic gradient (the first two terms on the right-hand side of (4)) away from the margin is close to $\rho_w g \sin\alpha = 362$ Pa m^{-1}, steepening towards the margin. With $u_b h = 3$ m^2 year^{-1}, the critical discharge Q_c can then be estimated as 0.22 m^3 s^{-1}. The mean discharge per conduit for each simulation is listed in table 2. This shows that the case $m = 1$ cm day^{-1}, at which we first observe spontaneous channelization, therefore corresponds closely to a mean discharge per conduit close to the critical flux Q_c. Exact agreement of course cannot be expected: a number of simplifying assumptions in section 2 do not hold here, such as a fixed hydraulic gradient or perfectly laterally connected conduits. In addition, the conduit network also exhibits the hysteresis shown in figure 5: as discussed, channelized as well as unchannelized drainage system can exist stably for $m = 0.66$ cm day^{-1} and 1 cm day^{-1}. Panels (c) and (d) of figure 2 in the main text also show the transitions from unchannelized to channelized systems.

4 Effective pressure dependence on discharge

4.1 Dependence on mean discharge in steady state: conduits in parallel

The main interest in subglacial drainage is its effect on ice dynamics through effective pressure: this is the variable through which water at the glacier bed enters into the sliding motion of ice. At the simplest level, we are interested in a relationship between water input as a forcing and effective pressure as a response.

For a fixed number of drainage conduits (for instance, fixed by bed protrusions allowing ice-bed gaps to form), a given water input translates into a given mean discharge $\bar{Q}$ per conduit. If $\bar{Q} < Q_c$ and drainage is distributed equally among the conduits, equation (31) (equation (2) in the main article) provides the relationship between effective pressure and discharge. Effective pressure decreases with increasing discharge before channelization (panel (a) of figure 5)

Once channelization occurs, effective pressure increases with discharge $\bar{Q}$ (see 40). Equation (31) however no longer holds: the discharge Q in an individual conduit is no longer equal to $\bar{Q}$ as flow has become concentrated. In the channels, $Q > \bar{Q}$. As effective pressure in channel conduits increases with discharge, $\bar{N}$ after channelization exceeds $\bar{N}$ in (31). For an array of conduits, panel (a) of figure 5 shows that the jump in $\bar{N}$ on channelization is bigger for larger n_c.

For all the n_c shown in figure 5, the jump in $\bar{N}$ on channelization remains modest: a big increase in $\bar{N}$ requires very many conduits to be channelized. To see this, note that (31) actually gives the correct relationship between effective pressure and

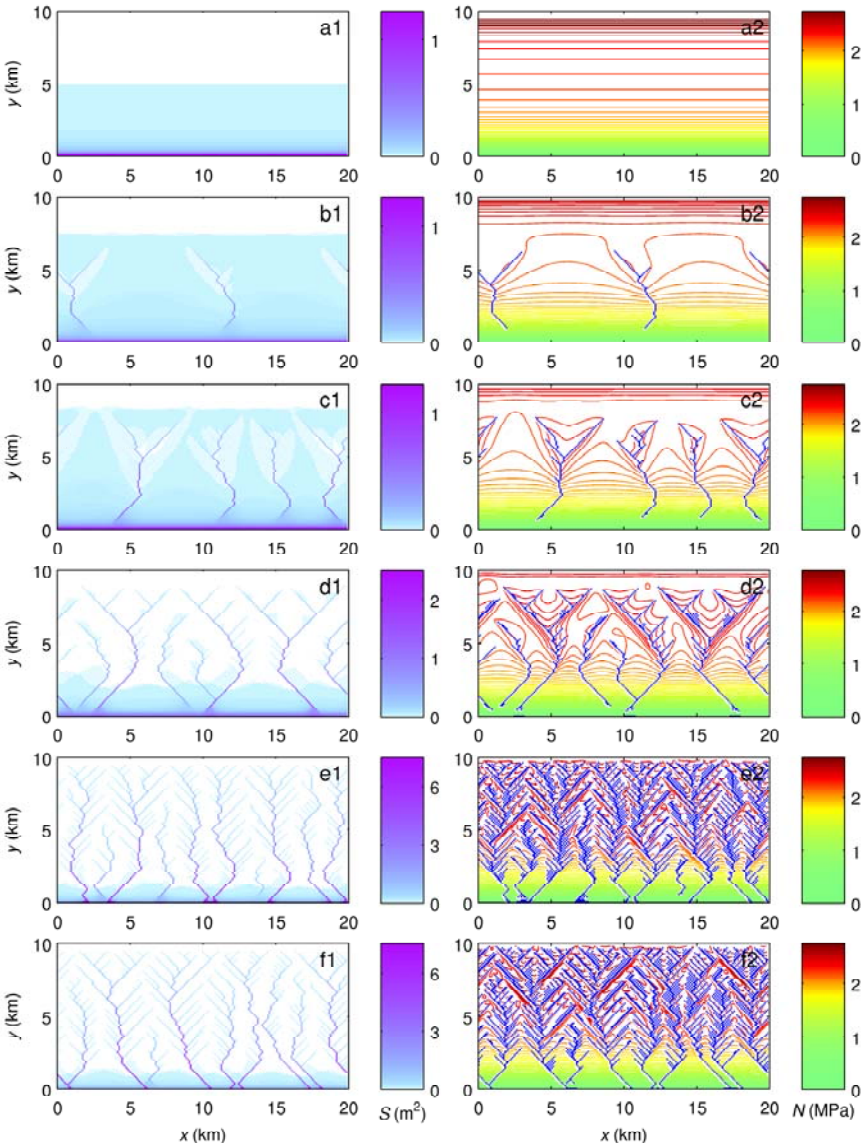


Figure 7: Steady state drainage network solutions. Left-hand column: steady-state conduit sizes. Right-hand column: corresponding effective pressure contours (0.05 MPa interval), channels shown as blue pixels. y is distance from the margin, x distance cross-glacier. Rows (a)–(e): simulations with zero water storage at the bed, wth m = 10 cm day^{-1} (e1,e2), 2 cm day^{-1} (d1,d2), 1 cm day^{-1} (c1,c2), 0.66 cm day^{-1} (b1,b2) and 0.33 cm day^{-1} (a1,a2). The simulations in (d1,d2) and (e1,e2) were started with nearly uniform initial conditions, with channels emerging through the unstable growth of small initial perturbations. (a1,a2), (b1,b2) and (c1,c2) were started with the configuration in (e1) as initial condition; no channels formed when these simulations were rerun with nearly uniform initial conditions. The evolution of the patterns in (e1,e2),(b1,b2) and (c1,c2) is shown in the animations `networkformation1.mpg`, `networkformation2.mpg` and `networkformation3.mpg`. Panels (f1,f2): same parameter values as (e1,e2) but with storage. The pattern produced is different in detail from (e1,e2) but qualitatively similar.

flux in *any* conduit in steady state if $\bar{Q}$ and $\bar{N}$ are interpreted as discharge and effective pressure in that conduit. For a big channel ($Q \gg Q_c$), I can approximate this relationship by dropping the $u_b h$ term, so that

$$N \sim [c_1 c_2^{-1} c_3^{1/\alpha}]^{1/n} \Psi^{(2\alpha+1)/(2n\alpha)} Q^{(\alpha-1)/(n\alpha)}. \tag{50}$$

With $n = 3$ and $\alpha = 5/4$, this gives $N \propto Q^{1/15}$. N barely changes at all with discharge for a channel: discharge has to incease by a factor of $2^{15} \approx 3 \times 10^4$ in order to double effective pressure, meaning that about $30,000$ conduits have to be channelized into a single big channel to double effective pressure compared with the prediction of (31) for the relationship between mean effective pressure and mean discharge.

4.2 Steady discharge in a network of conduits

A simple array model as in 2.1.2 cannot predict the number n_c of conduits that drain into a main channel in a real drainage system. The more elaborate network model of section 3.2 can do this. In figure 7, channel spacing in steady states decreases with water input (and hence with discharge). The number of conduits n_c draining into a main channel therefore decreases with mean discharge $\bar{Q}$. A real drainage system will not follow a single curve with fixed n_c in figure 5, but will transition from high n_c to lower n_c as $\bar{Q}$ increases: $\bar{N}$ increases less rapidly with $\bar{Q}$ than suggested by the curves for fixed n_c shown in figure 5. The hysteresis evident in figure 5 is however preserved by the network model (figure 2 of the main article and figure 7 here).

To determine the degree to which channelization raises effective pressure in a conduit network, I compute mean effective pressure $N_{\mathrm{av}}(y)$ in each cross-section (line of constant distance from the margin) for the drainage systems in figure 7. Figure 8 shows $N_{\mathrm{av}}(y)$ against y (discrete markers). Panel (d) of figure 2 in the main text also shows the dependence of the mean of effective pressure taken over the entire domain against water supply rate N. Both figures show that channelization causes modest changes in effective pressure (a jump of around 15 %). Panel (d) of figure 2 in the main text further confirms that effective pressure decreases with water supply rate (and hence discharge) for a stable unchannelized system, and increases with water supply for a channelized system. Note that the unchannelized system becomes unstable before the minimum mean effective pressure for an unchannelized system is reached. This is no contradiciton to the earlier results in section 28, and in particular in figure 5: the channelizing instability only requires that the critical discharge Q_c is reached locally in a conduit in the network. In the more complicated geometry of our network, this can happen before the minimum mean effective pressure is reached.

As described above, the degree of channelization (how many smaller conduits n_c feed into a large channel-like conduit) controls the jump in effective pressure on channelization. The larger n_c, the more discharge Q in the channel exceeds $\bar{Q}$, and the more $\bar{N}$ will exceed the prediction of (31). The degree of channelization is equivalent to the spacing between channels, as the smaller conduits in between will feed into these channels. Although my model can predict channel spacing numerically (see panel (c) of figure 2 in the main text), a qualitative understanding would be useful. Lateral

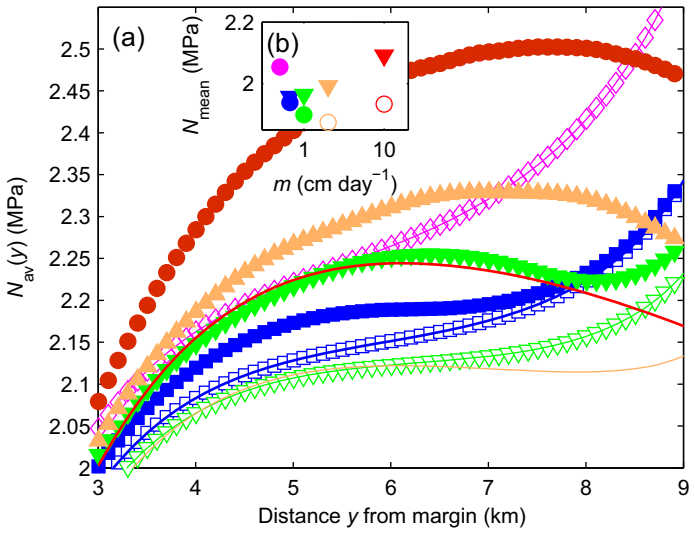


Figure 8: Effective pressure changes due to channelization. (a): Steady state mean effective pressure $N_{av}(y)$ at distance y from the glacier margin for different water input rates m (= 0.5 cm day^{-1} (magenta), 0.66 cm day^{-1} (blue), 1 cm day^{-1} (green), 2 cm day^{-1} (orange) and 10 cm day^{-1} (red)). Solid curves show the relationship for unchannelized systems, which are stable when shown with empty markers, and unstable when without markers. At low m, an increase in water input leads to effective pressure decreasing (magenta to blue to green), and the unchannelized system remains stable. Subsequently, effective pressure increases again, and the unchannelized system becomes unstable (green to orange to red). In stable unchannelized systems, $N_{av}(y)$ generally decreases as the margin is approached because discharge increases towards the margin. By contrast, unstable unchannelized systems generally have a region in which $N_{av}(y)$ increases as the margin is approached (e.g. at $y = 7.5$ km on the orange line). Hence there is a region in which effective pressure increases with discharge, which is predicted to lead to instability in section 28. The solid markers show N_{av} for channelized systems. In these, N_{av} generally increases with water input (blue to green to orange to red), and exceeds effective pressure in the unchannelized system. For some intermediate water supply rates, both channelized and unchannelized systems are possible (blue, green), showing that the drainage system can have multiple stable states. (b): Hysteresis. Mean effective pressure N_{mean} over the whole domain against m. Full circles are stable unchannelized systems, empty circles unstable unchannelized systems. Triangles are channelized systems. Effective pressure decreases with water supply before channelization, jumps to a higher value upon channelization (by about 20 %) and increases with water supply thereafter. Channelization is also irreversible: it first occurs close to $m = 1$ cm day^{-1}, but can persist down to between $m = 0.5$ and 0.66 cm day^{-1}.

pressure gradients are clearly important: in their absence, neighbouring channels would be subject to the same effective pressure N, and the stability analysis above would predict the formation of a single channel.

Between each of the channels in figure 7, there is an effective pressure trough (water pressure ridge) that drives water towards both of the neighbouring channels, and prevents water leaking from one channel into the other. A simple length scale argument shows that this leads to closer channel spacing at higher discharge. (This is similar to the compaction length arguments in recent work by Hewitt[23,24] based on an analogy with models for compaction of partial melts.)

The argument runs as follows: my computations suggest that channels are separated by a region of cavities with effective pressure lower than in either of the channels, so that water cannot drain from one channel through the cavity region into the other channel. This effective pressure low is associated with the lateral drainage of water supplied to the cavities into the adjacent channels. Let m be the rate of water input per unit area of bed and let the conduit spacing in the network be L, so that the channel spacing becomes $L_c = n_c L$. The discharge in each cavity then scales as mLL_c. This lateral drainage is driven by a lateral pressure gradient $\Psi \sim \Delta N/L_c$. If this lateral pressure gradient creates an effective pressure low between two channels, then ΔN must scale with the pressure difference ΔN_c between the channels, so $\Psi \sim \Delta N_c/L_c$. But the discharge in the cavities can be approximated as

$$Q \sim mLL_c \sim c_3 S^\alpha \Psi^{1/2} \sim c_3 S^\alpha (\Delta N_c/L_c)^{1/2}. \tag{51}$$

However, in the cavities I have from (10)

$$S \sim \frac{u_b h}{c_2 N_c^n}, \tag{52}$$

where N_c is a scale for effective pressure, and so

$$mLL_c \sim c_3 \left(\frac{u_b h}{c_2 N_c^n}\right)^\alpha \left(\frac{\Delta N_c}{L_c}\right)^{1/2}. \tag{53}$$

The difference in channel pressure ΔN_c and channel pressure N_c can also be approximated by noting that channel pressure $N_c = N_c(Q_c)$ is a function of channel discharge Q_c through (50), and $\Delta N_c \sim N_c'(Q_c)\Delta Q_c \sim N_c'(Q_c)Q_c$ if we allow an order one difference $\Delta Q_c \sim Q_c$ in discharge between neighbouring channels; from (50), $N_c'(Q_c)Q_c$ is given by

$$\Delta N_c \sim N_c'(Q)Q = \frac{\alpha - 1}{\alpha n} N_c = \frac{1}{15} N_c \tag{54}$$

if $\alpha = 5/4$ and $n = 3$. (Note that this is reasonable: in figure 7, I have $N_c \approx 2.2$ MPa, so $N_c/15 \approx 0.15$ MPa. The local lows in N between channels correspond to a few contour lines, which are spaced at 0.05 MPa, so ΔN_c is a little larger than 0.05 MPa.) Substituting and rearranging gives us the channel spacing L_c as

$$L_c \sim c_3^{2/3} c_2^{-2\alpha/3} \left(\frac{\alpha - 1}{\alpha n}\right)^{2/3} L^{-2/3} m^{-2/3} (u_b h)^{2\alpha/3} N_c^{(1-2\alpha n)/3}, \tag{55}$$

One can check that this gives appropriate scalings: for $m = 10$ cm day^{-1} and $m = 2$ cm day^{-1} with the parameter values defined in section 3.2, (55) gives spacings of 130 m and 400 m; this is somewhat less than panels a2 and b2 of figure 7 would suggest but is reasonable. Moreover, the qualitative behaviour of (55) is in agreement with figure 7: L_c decreases with increasing water input rate m and channel pressure N_c (which itself increases with water input rate). Clearly more research is needed to investigate controls on channel spacing in detail, and there are numerous complications one could consider, such as secondary channels between the main ones. However, the above indicates a reasonable starting point for such an investigation.

4.3 Localized water input

The computations above were based on a spatially uniform water input. Water is supplied equally to all network nodes. In real glaciers, water is channeled to the bed via discrete moulins and crevasses whose spacing is likely to be larger than the conduit spacing set by bedrock roughness (i.e., the node spacing in our network model). To test sensitivity to localized water input, I have also run simulations in which water is supplied at a spatially uniform background rate of $m_0 = 0.33$ m day^{-1}, and in addition at a higher rate Δm_i to N_{rand} randomly located nodes. A mean water supply rate can then be defined as

$$m = m_0 + \Delta m_i N_{\text{rand}} / A_{\text{domain}}. \tag{56}$$

The dependence of steady-state channel density and mean effective pressure N_{mean} on m for one particular set of randomly located nodes is shown in figure 9, analogous to figure 2 (c) and (d) of the main text. The behaviour of the system remains qualitatively the same, but several quantitative differences are clear. Firstly, the initial drop in effective pressure with increasing m, which occurs at low m, is less steep for localized water supply (panel (b)). Moreover, a few widely spaced channels are present even at these low m (panel (a)). This is the result of very localized water input leading to the formation of short channels that then leak into the surrounding cavities and peter out. Secondly, the onset of large-scale channelization occurs earlier for localized water input: it is easier to gather enough water to form a channel if water is supplied unevenly. The resulting jump in N_{mean} and subsequent increase with increasing m is also more pronounced (panel (b)), while channel density remains lower than for uniform water supply. The cavities between channels carry less water for localized water input, concentrating water in the channels and leading to higher effective pressure. Moreover, channels are not required to carry water away from nodes that receive only the background rate of water supply. The tendency for the drainage system to exhibit hysteresis is also suppressed. Hysteresis occurs because channels can sustain themselves by drawing in water from the surrounding cavities due to their lower water pressure. This ability to sustain themselves is however lessened when only very little water is supplied to these surrounding cavities.

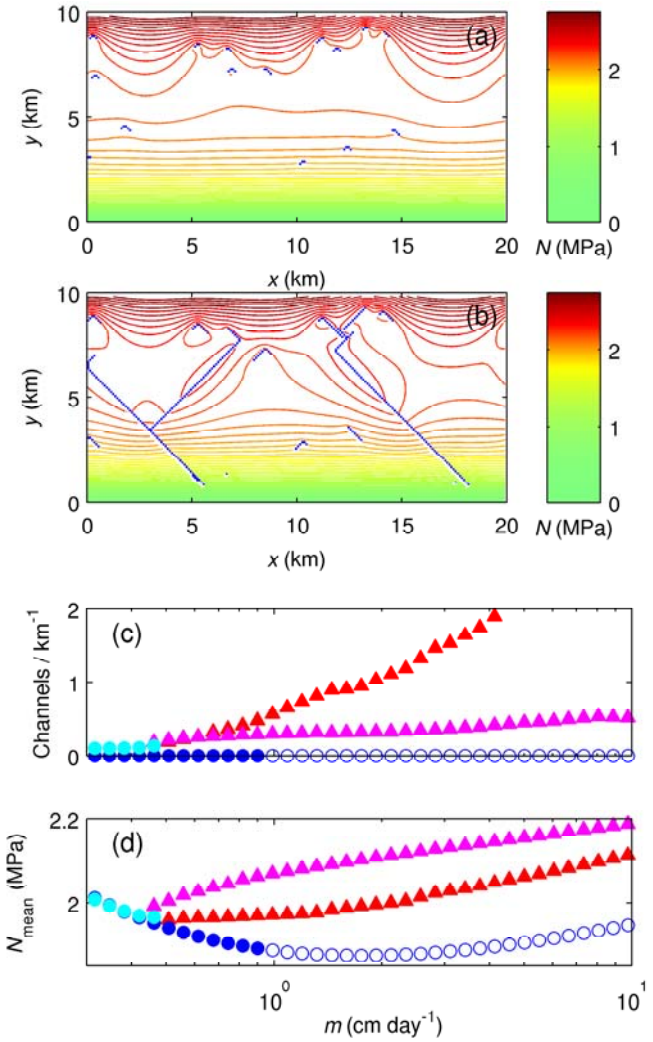


Figure 9: Steady state drainage networks with localized water input. Analogous to figure 2 in the main text, but showing data for networks with localized water input as described in section 4.3. Panels (a) and (b) show effective pressure and channelized conduits in a system with twenty randomly located nodes receiving localized water input, with $m = 0.42$ cm day^{-1} (panel a) and $m = 0.51$ cm day^{-1} (panel b). Panels (c) and (d) still show channel density and mean effective pressure as functions of water supply rate m. Blue and red markers in panels (c) and (d) refer to systems with spatially uniform water supply, with blue showing unchannelized systems (full circles are stable, empty circles unstable) and red showing channelized systems. Cyan and magenta correspond to systems with nonuniform water input. Cyan circles are stable 'unchannelized' systems, magenta triangles are stable channelized systems. By 'unchannelized' we mean here that each node receiving a higher rate of water input has only localized channels attached, which do not extend significantly across the domain (see panels (a) and (b)).

5 Temporal variations in water input

5.1 Seasonal drainage system evolution

Recent observations in Greenland by Bartholomew *et al.*[25] have shown that the seasonal evolution of the drainage system there can lead to a period of faster ice flow that lasts several weeks early in the melt season. These results are compatible with our model as shown by figure 3 of the main text and in figure 10 here.

In the simulation in figure 10, the system starts at low water supply rates in an unchannelized state (panel (c)). An initial increase in water supply at the beginning of the summer season has a similar effect to the increases in water supply in figure 11, and leads to an abrupt increase in water pressure. This is the 'spring event'[26] in figure 10. The corresponding drop in effective pressure causes all conduits in the system to widen (S_{mean} increases). However, as the system is initially not channelized (panel (d)), effective pressure then remains lower than at wintertime water supply levels in order to maintain the conduits open. Eventually, channelization becomes pronounced (panels (e) and (f)), corresponding to a decrease in mean conduit size but an increase in variance in conduit size (panel (b)). The system eventually returns to an unchannelized state when water supply is reduced at the end of the summer season (panel (g)).

These results indicate that the length of time taken by the channelization process explains the long period of somewhat increased ice velocities in the observations of Bartholomew *et al.* However, the potential of the seasonal switching in drainage to cause ice flow speedup is limited. As shown in figure 4 of the main text, the length of time taken to channelize is reduced with increasing meltwater input in summer. Moreover, the drop in effective pressure *after* the spring event compared with wintertime pressures is also reduced at higher summer meltwater input. This implies that stronger, steady summer melting alone will not necessarily cause faster average ice velocities.

5.2 Short-term variations in water input

In addition to the slow seasonal evolution of the drainage system, short time scale variations in water input can have a very significant effect on effective pressure, causing excursions from its steady state value. This is important over short time scales, on which conduit size cannot respond to changes in input.

Consider input Q varying on these time scales. If I treat conduit size S as constant, changes in discharge $Q(t)$ must therefore be accomodated by changes in hydraulic gradient:

$$\Psi(t) = c_2^{-2} S(t)^{-2\alpha} |Q(t)| Q(t). \tag{57}$$

Recall that Ψ is composed of a geometrically controlled mean hydraulic gradient Ψ_0 and an effective pressure gradient $\partial N/\partial s$, where s is distance down-conduit (see equation (4)). When Q increases, hydraulic gradient therefore also increases. This can only occur through an increase in effective pressure gradient $\partial N/\partial s$ toward the glacier margin. This implies that effective pressure N must drop in the interior of

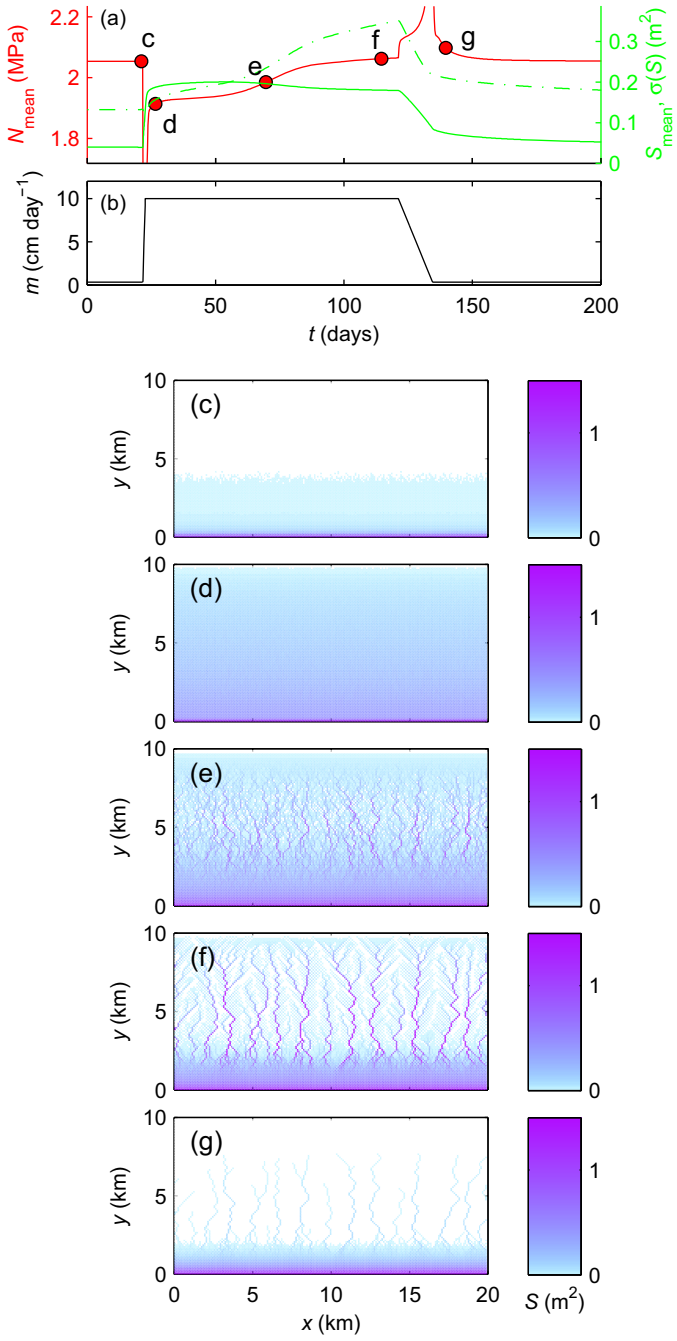


Figure 10: Idealized seasonal evolution of the drainage system. This figure is analogous to figure 4 in the main text. (a): The spatial mean of effective pressure N_{mean} (red line) against time. The green lines show mean conduit size S_{mean} (solid line) and standard deviation $\sigma(S)$ (dot-dashed line) of conduit size over the domain as functions of time. (b) The simulation shown is forced by the melt supply rate $m(t)$ shown as a black line. The dots marked c, d, e, f and g correspond to the spatial drainage system configurations shown in panels (c), (d), (e), (f) and (g) respectively. (b) . An increase in $\sigma(S)$ at time when S_{mean} is constant or decreasing indicates channelization of the system. A video animation is available in `seasonalevolution.mpg`

the glacier, which corresponds to a basal water pressure spike away from the margin. Similarly, effective pressure in the interior of the glacier will rise when Q is reduced.

This is evident in the simulations of abrupt drainage events in figure 11 (also figure 4 of the main text). A short-lived, sharp increase in water supply to the glacier leads to an abrupt increase in flux, which can be accomodated only by the rise in Ψ and hence the drop in effective pressure described above. This remains true even when water storage is allowed for, so that the increase in water input does not translate instantly into an increase in water storage. The water pressure spike is only transient, as channels then begin to widen and are able to accomodate more discharge at lower Ψ. When water input is reduced again, the channels are now wider than necessary and the reduced discharge causes a drop in Ψ, corresponding to a peak in effective pressure.

To understand better how this affects sliding velocity, I use a simple sliding law[26,27,7] of the form

$$\tau_b = C u_{\text{slide}}^{1/p} N \tag{58}$$

where τ_b is shear stress at the bed, u_{slide} is the modelled sliding velocity, and C and p are constant model parameters. In general, τ_b, u_{slide} and N depend on both, time and position. For simplicity, I assume that there are no significant variations in sliding velocity over the domain, with stresses in the ice maintaining an approximately uniform ice velocity. Then u_{slide} can be treated as constant over the domain. I also assume that the spatial mean over shear stress at the bed equals the gravitationally defined driving stress acting on the ice.[7] If the subscript 'mean' denotes a spatial average over the domain at a fixed time t, then

$$\tau_{b,\text{mean}} = C u_{\text{slide}}^{1/p} N_{\text{mean}}, \tag{59}$$

or

$$u_{\text{slide}} = C^{-1} \tau_{b,\text{mean}}^{p} N_{\text{mean}}^{-p}. \tag{60}$$

Assuming further that the glacier geometry does not change during a drainage event, the change in modelled sliding velocity during these events can be normalized to the steady state velocity prior to the event. Denoting this velocity by

$$u_0 = C^{-1} \tau_{b,\text{mean}}^{p} N_{0,\text{mean}}^{-p}, \tag{61}$$

where N_0 is the steady state effective pressure distribution, we have

$$\frac{u_{\text{slide}}}{u_0} = \frac{N_{0,\text{mean}}^{p}}{N_{\text{mean}}^{p}}. \tag{62}$$

Panel c of figure 4 of the main text shows time series of u_{slide}/u_0 for various values of p. Figure 11 shows corresponding temporal averages of u_{slide}/u_0 against the parameter p. Note that we treat u_{slide} as a passive quantity that does not couple back into the drainage system; a better model would be to equate $u_b = u_{\text{slide}}$ but the calculation here gives a rough idea of the ice flow response to short term drainage events.

Clearly, this response is more pronounced for larger p, but in all cases, the temporal average of u_{slide} exceeds the steady state velocity u_0: the effect of the initial drop

in effective pressure in speeding up ice flow dominates over the effect of the later spike in effective pressure slowing down ice flow. Moreover, most glacier sliding laws derived from first principles[27,11,12] predict that shear stress τ_b depends weakly on sliding velocity, suggesting large values of p. This then indicates that episodes of low effective pressure have a disproportionate effect on glacier sliding compared with high effective pressure episodes as suggested by figure 4 of the main text, and a significant speedup during short term drainage events. Note however that the calculation above is too simplistic in that it assumes the driving stress on the domain to be supported fully by the bed. In practice, during episodes of low N, stress transfer away from the area would suppress excessively large sliding velocities. In particular, a fractional increase in mean sliding velocity of 10^2 as suggested for $p = 10$ is clearly not realistic.

In the simulations in figure 11 (see also the video animations `drainageevents1.mpg` and `drainageevents2.mpg`), water input was increased everywhere during the drainage events shown. The video animation `drainageevents3.mpg` shows a simulation in which water supply rate is increased to fifty times the background value over a randomly chosen area measuring 0.1 km^2 at random times (indicated by red dots in the animation). As in figure 11, these drainage events are modelled to last 5 days. A similar pattern of an initial drop in effective pressure followed by an increase is observed in these simulations, but the effect is more localised to the catchment areas of the main drainage channels in which the drainage events occur.

Clearly, the pressure response of the drainage system to water input variations depends on the timescale of variability, as a comparison of figures 11 and 10 demonstrates. To understand this more systematically, I have also performed computations using the solution in (e1) of figure 7 as an initial condition, and imposing variations in water input as

$$m(t) = m_0 + \Delta m \sin(2\pi t/T), \tag{63}$$

where $m_0 = 10$ cm day^{-1} and $\Delta m = 8$ cm day^{-1}, and the period of oscillation T is changed between simulations. The response of the drainage system is shown in figure 12 for $T = 1$ day, 7 days, 30 days and 365 days. As an initial condition, I have used the solution shown in row e of figure 7, which is a steady state for m_0. The system is then evolved forward until it exhibits periodic oscillations.

For short periods T, water supply and effective pressure are out of phase: water supply maxima correspond to water pressure maxima and hence effective pressure minima as conduit size is unable to adjust significantly during a single period, and the additional water flow must be accomodated by increased hydraulic gradients. Correspondingly, the amplitude of mean effective pressure variations is also biggest for these high-frequency oscillations, while variations in mean conduit size and in the standard deviation of conduit size (indicating changes in the degree of channelization) are small. For long periods, water supply becomes increasing in phase with effective pressure: the system remains more closely in a quasi-steady state. For such a quasi-steady state in a channelized system, increased discharge corresponds to increased effective pressure. In addition, variations in effective pressure become more modest as the system adjusts readily to admit more or less discharge, and large variations in hydraulic gradient are not required.

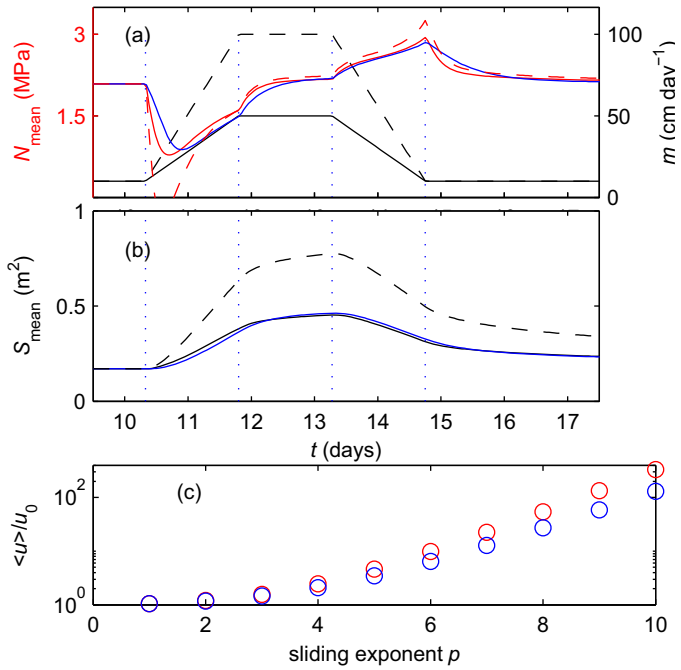


Figure 11: Temporal variations in water input. This figure is analogous to figure 4 in the main text. (a): The mean of N taken over the domain against time (red and magenta). Simulations are started with the solution in (e1) of figure 7 as initial condition. The solid and dashed lines correspond to the water supply forcing shown by solid and dashed black lines in panel (a), respectively. The red lines correspond to no storage at the network nodes, magenta line corresponds to the same forcing parameters as the solid line, but has storage at the network nodes described by (48) with $u_b h_v L_V = 835$ m^3 day^{-1}. (b): The mean of conduit size S against t, solid and dashed lines again correspond to the solid and dashed melt supply curves shown in black in panel (a). Theblue lines shows that storage at the bed has a quantitative but not qualitative effect on transient drainage response. (c): A temporal average over u_{slide}/u_0 s defined in (62) for various values of the sliding law parameter p, for the simulation corresponding to the solid $m(t)$ curve in panel (a). Red circles correspond to no storage, blue circles to water storage. In both cases and for all p, the temporal average of u_{slide} exceeds the steady state velocity u_0. The response is much more pronounced for larger values of p. Video animations of the drainage response shown here are available in `drainageevents1.mpg` and `drainageevents2.mpg`

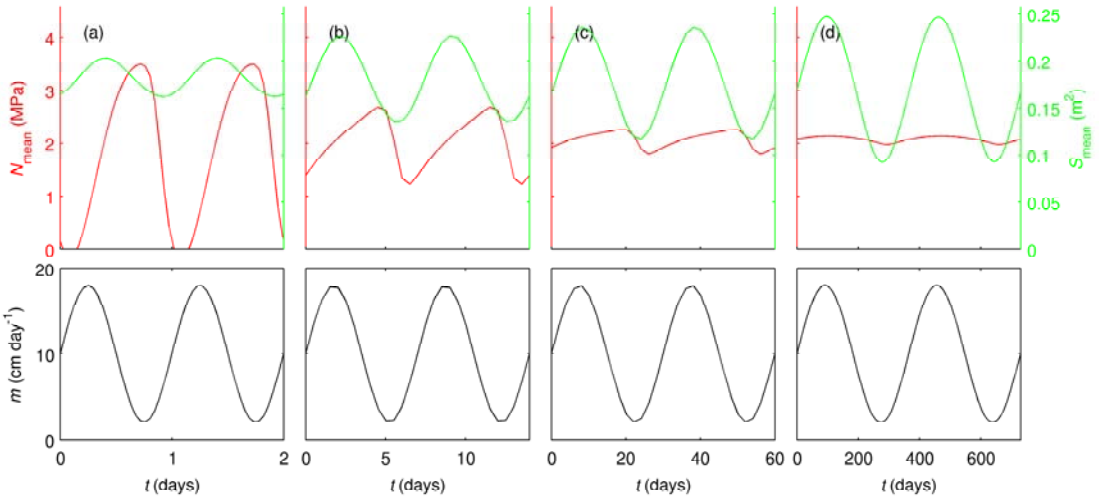


Figure 12: Drainage system response to sinusoidal forcing of different frequencies. Top row: time series of mean effective pressure (red), mean conduit size (green). Bottom row: the corresponding sinusoidal water input forcing time series. Column (a) has a period of $T = 1$ day, (b) has $T = 7$ days, (c) has $T = 30$ days, (d) has $T = 365$ days

These simulations confirm what the simulations of seasonal and short term water input variations in the main text have already indicated: Large effective pressure variations leading to temporary speedup are mostly generated by short term water input variations, while slow secular increases in water supply tend to lead to channelization and slowdown.

References

1. Hubbard, B. and Nienow, P. Alpine subglacial hydrology. *Quat. Sci. Rev.* **16**, 939–955 (1997).

2. Fountain, A.G. and Walder, J.S. Water flow through temperate glaciers. *Rev. Geophys.* **36**(3), 299–328 (1998).

3. Walder, J. Hydraulics of subglacial cavities. *J. Glaciol.* **32**(112), 439–445 (1986).

4. Röthlisberger, H. Water pressure in intra- and subglacial channels. *J. Glaciol.* **11**(62), 177–203 (1972).

5. Nye, J.F. Water flow in glaciers: jökulhlaups, tunnels and veins. *J. Glaciol.* **17**(76), 181–207 (1976).

6. Nye, J.F. The flow law of ice from measurements in glacier tunnels, laboratory experiments and jungfraufirn borehole experiments. *Proc. R. Soc. Lond. A* **219**(1139), 477–489 (1953).

7. Paterson, W.S.B. *The Physics of Glaciers*. Pergamon, Oxford, 3rd edition, (1994).

8. Clarke, G.K.C. Lumped-element analysis of subglacial hydraulic circuits. *J. Geophys. Res.* **101**(B8), 17547–17559 (1996).

9. Fowler, A.C. A sliding law for glaciers of constant viscosity in the presence of subglacial cavitation. *Proc. R. Soc. Lond. A* **407**, 147–170 (1986).

10. Kamb, B. Glacier surge mechanism based on linked cavity configuration of the basal water conduit system. *J. Geophys. Res.* **92**(B9), 9083–9100 (1987).

11. Schoof, C. The effect of cavitation on glacier sliding. *Proc. R. Soc. Lond. A* **461**, 609–627, doi:10.1098/rspa.2004.1350 (2005).

12. Gagliardini, O., Cohen, D., Raback, P., and Zwinger, T. Finite-element modeling of subglacial cavities and related friction law. *J. Geophys. Res.* **112**(F2), F02027, doi:10.1029/2006JF000576 (2007).

13. Weertman, J. General theory of water flow at the base of a glacier or ice sheet. *Revs. Geophys. Space Phys.* **10**(1), 287–333 (1972).

14. Lliboutry, L. General theory of subglacial cavitation and sliding of temperate glaciers. *J. Glaciol.* **7**(49), 21–58 (1968).

15. Fowler, A.C. Breaking the seal at Grimsvötn. *J. Glaciol.* **45**(151), 506–516 (1999).

16. Creyts, T.T. and Schoof, C.G. Drainage through subglacial water sheets. *J. Geophys. Res.* **114**(F04008), doi:10.1029/2008JF001215 (2009).

17. Kramer, S. and Marder, M. Evolution of river networks. *Phys. Rev. Lett.* **68**(2), 205–208 (1992).

18. Murray, A.B. and Paola, C. A cellular model of braided rivers. *Nature* **371**, 54–57 (1994).

19. Ng, F.S.L. Mathematical modelling of subglacial drainage and erosion, (1998). *http://www.maths.ox.ac.uk/research/theses/*.

20. Kamb, B., Raymond, C.F., Harrison, W.D., Engelhardt, H., Echelmeyer, K.A., Humphrey, N., Brugman, M.M., and Pfeffer, T. Glacier surge mechanism: 1982–1983 surge of Variegated Glacier, Alaska. *Science* **227**(4686), 469–479 (1985).

21. Flowers, G.E. and Clarke, G.K.C. A multi-component model of glacier hydrology. *J. Geophys. Res* **107**(2287), doi:10.1029/2001JB001122 (2002).

22. Nye, J.F. The flow of glaciers and ice-sheets as a problem in plasticity. *Proc. R. Soc. Lond. A* **207**(1091), 554–572 (1951).

23. Hewitt, I.J. *Mathematical modelling of geophysical melt drainage*. PhD thesis, Oxford University, (2009).

24. Hewitt, I.J. and Fowler, A.C. Melt channelization in ascending mantle. *J. Geophys. Res.* **114**(b06210), doi:10.1029/2008JB006185 (2009).

25. Bartholomew, I., Nienow, P., Mair, D., Hubbard, A., King, M.A., and Sole, A. Seasonal evolution of subglacial drainage and acceleration in a Greenland outlet glacier. *Nature Geoscience* **3**, 408–411 (2010).

26. Iken, A. and Bindschadler, R.A. Combined measurements of subglacial water pressure and surface velocity of Findelengletscher, Switzerland: conclusions about drainage system and sliding mechanism. *J. Glaciol.* **32**(110), 101–119 (1986).

27. Fowler, A.C. Sliding with cavity formation. *J. Glaciol.* **33**(105), 255–267 (1987).